Hindawi
International Journal of Optics
Volume 2023, Article ID 6652333, 12 pages
https://doi.org/10.1155/2023/6652333

Research Article

Refractometric Sensing of Protein in Urine by the Photonic Crystal Fiber Biosensor in THz Regime

Md. Moshiur Rahman,[1] **Farhana Akter Mou**,[1] **Mohammed Imamul Hassan Bhuiyan**,[2] **and Mohammad Rakibul Islam**[3]

[1]*Department of Electrical & Electronic Engineering, University of Asia Pacific, Dhaka, Bangladesh*
[2]*Department of Electrical & Electronic Engineering, Bangladesh University of Engineering and Technology, Dhaka, Bangladesh*
[3]*Department of Electrical & Electronic Engineering, Islamic University of Technology, Gazipur, Dhaka, Bangladesh*

Correspondence should be addressed to Md. Moshiur Rahman; sourov.eee042@gmail.com

Received 3 June 2023; Revised 22 September 2023; Accepted 17 October 2023; Published 26 October 2023

Academic Editor: Li-Ming Si

The presence of albumin in human urine is one of the confirmed early symptoms of kidney dysfunction. A precise urine protein identification process is very important to monitor the kidney's proper functioning. To identify the presence of albumin in urine, a refractometric protein sensing approach in the photonic crystal fiber (PCF) environment has been introduced here. A PCF geometry with suspended cladding and a circular hollow core has been proposed and investigated in the terahertz (THz) spectrum for protein identification in the liquid samples. Three levels of albumin concentrations in urine (7–125 mg/dl, 250–500 mg/dl, and 1000 mg/dl) are considered to evaluate the sensing performances of the proposed PCF. The numerical investigations are performed on the COMSOL Multiphysics platform where the finite element method (FEM) figures out the numerical outcomes. The performances of the proposed PCF exhibit highly sensitive characteristics for albumin identification in the different albumin concentration levels of urine. The sensitivity shows more than 98.5% for all the tested concentration levels due to the strategic selection of geometrical parameters and proper optimization. Alongside, negligible confinement loss of 10^{-16} cm^{-1} is attained at the same operating point of 4.3 THz. Furthermore, dispersion profiles and practical implementation strategies are also investigated and discussed in detail.

1. Introduction

The kidneys are the vital organ in the body located in the back on either side of the vertebral column. These two bean-shaped organs are responsible for getting rid of waste products, drugs, and toxins through urine, balancing the body's fluids, controlling the production of red blood cells, producing an active form of vitamin D, etc. So, maintaining kidney health is very significant because its performance disturbance creates an overall health disorder and even may lead to death. Regular monitoring of the kidney's functionality is very urgent because there are no visible symptoms of kidney disorders until they are damaged. If the kidney disorder can be traced and treated early, it may be possible to stay away from any kind of worse. A blood creatinine or urine protein test can assess the kidneys' functioning situations [1, 2].

Normally, albumin is present in the blood. The kidneys filter the blood to conserve the blood proteins and dispel waste products. The waste products are closed in urine, and the blood proteins like albumin stay in the blood vessels. If the presence of albumin is found in the urine, it definitely is an initial sign of a kidney's abnormality that is called albuminuria or proteinuria. The functioning situation inside a healthy kidney and albuminuria conditions are displayed in Figure 1. This figure interprets that when the kidneys are performed properly, virtually no albumin is leaked into the urine. On the contrary, if the kidneys end up damaged or

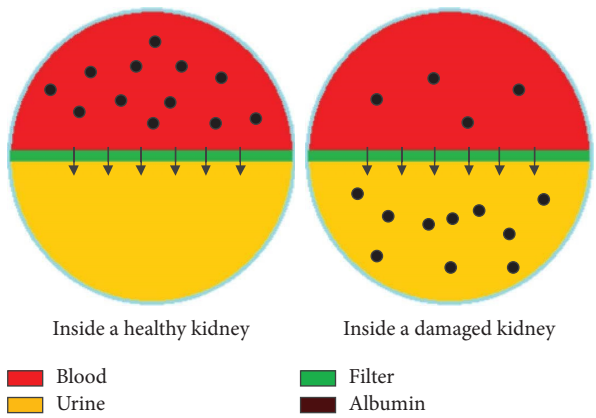

Figure 1: Albumin filtering situation inside a healthy kidney and an infected kidney.

diseased, they will lose their competence to conserve albumin. So, albumin identification in the urine can be an effective way to trace an early kidney infection.

An incredible pace in the sensor field has emerged in the modern photonic technology after the invention of novel photonic crystal fiber (PCF). Recently, PCF has proved its potential in the sensing platform due to its highly promising guiding features, versatile diversity for applications, and faster response with precise results for detection approaches, which are an insurmountable difficulty for conventional optical fiber. The most remarkable acquisition of the PCF sensor is that it allowed greater freedom for geometrical arrangement. The optical behaviors of PCF biosensor can be modified for precise functioning by tuning the geometrical parameters such as the pattern, size, and shape of air holes [3, 4]. In addition, the PCF sensor has achieved the highest level of acceptance due to the higher sensitivity, small size, low cost, robustness, and more flexibility [5–8]. Furthermore, SPR-based PCF biosensor has a good potential for detecting biological components with high accuracy [9–14]. For these attractive features and precise level of performance, the PCF sensor has already shown evidence of its potentiality by furnishing the versatile strategies for applications in the sensing field such as chemical sensing [15], gas sensing [16], biosensing [17], RNA and DNA analysis [18, 19], genetic diagnostics [20], cancer diagnosis [21], humidity and temperature sensing [22, 23], as well as for low-loss waveguiding [24, 25] in the terahertz range. Terahertz technology already has shown numerous breakthroughs in various fields, especially biological sensing and it allows the measurement of dispersion and losses [6, 7, 7–15, 24, 25]. Highlighting the unparalleled features of this highly active area of science, we focused on developing rapid and convenient biosensors, considering the existing challenges and strategies.

Already, several pieces of research have been able to prove the potentiality of PCF devices in biosensing applications. Ahmed et al. designed a PCF geometry for blood constituent detection [7]. Nearly 80% sensitivity is achieved for all the tested blood components with negligible confinement loss. Another PCF structure has been proposed by Hossain and Podder [26] for blood component identification in the THz regime. This proposed hollow core geometry attained more than 90% sensitivity for RBCs, plasma, WBCs, hemoglobin, and water detection cases. Elhelw et al. proposed a PCF-based biosensor for blood bilirubin detection in the THz platform. A high-sensitive performance has been attained from the proposed PCF sensor with 98% sensitivity [27]. A topas-based PCF biosensor for blood cells detection has been proposed by Kumar et al. [28]. Glucose, plasma, WBC, and RBC have been considered as targeted analytes to evaluate the performance of their proposed decagonal solid-core PCF sensor. Almost 90% sensitivity is achieved for all the tested cases. A PCF biosensor has been proposed by Chopra et al. [29] for detecting molecules in biological samples and identifying different diseases. Cancerous cells, diabetes-affected cells, and different blood constituents are effectively identified in this work. A hexa-sectored square photonic crystal fiber sensor has been proposed by Assaduzzaman et al. for blood serum and plasma identification [30]. The proposed PCF sensor renders highly sensitive performance for both analyte identification cases with extremely low confinement loss and higher birefringence. For detecting the blood cholesterol, an octagonal-shaped hollow core-structured PCF has been presented by Rahman et al. [31]. Their developed PCF biosensor renders significant improvements in biological substance detection. Their proposed PCF attained 98.75% sensitivity for cholesterol detection in the THz spectrum that indicates the PCF devices have a huge potential in biosensing areas. The research works discussed above have some drawbacks such as improper core-cladding geometry, use of complex core-cladding structure, absence of crucial optical properties evaluation, higher losses, and lower sensitivity, whereas in general the issue of fabrication for practical implementation is not properly elaborated. Thus, there is ample scope to improve the performance of PCF through proper geometry selection and a simpler core-cladding structure. Besides, to the best of our knowledge, protein detection in urine concentration by a PCF sensor in the THz spectrum was not investigated before. Since PCF devices have been shown to be effective in the detection of various biological elements, there is a huge potential to develop a fabrication-friendly PCF platform with a high detection capability of protein in urine.

In this article, a circular hollow core PCF geometry has been proposed for protein detection in urine which will be applicable to identify the early kidney's dysfunctions. This proposed PCF geometry is investigated in the THz spectrum by adding different levels of albumin concentration in urine. The sensing performances of the proposed PCF render more than 98.5% sensitivity with an extremely low confinement loss of $10^{-16}\,\mathrm{cm}^{-1}$ at 4.3 THz operating conditions. A fabrication-friendly PCF structure development that is applicable for biosensing applications through proper design optimization that can identify the presence of protein in urine with higher sensitivity and low losses is the key aim of this research.

2. Design Methodology of the Proposed PCF Geometry

Considering the dominance profile of the PCF platform for chemical sensing, evanescent substances, and biological detection, several PCF geometries have been proposed over

the last decades. Square [32], circular [7], hexagonal [33], rhombic [34], pentagonal [35], octagonal [36], etc., have been developed and tested for different substances identification in the THz spectrum. The performance of existing PCF in sensing cases indicates that microstructured fiber can be a potential solution for sensing applications. The sensing performances of PCF devices are mostly dependent on geometrical arrangements. The geometrical arrangements of the proposed PCF are displayed in Figure 2 with the amplified view of the core, and the 3D view of developed PCF is presented in Figure 3 for better visualization. A horse-wheel-like, simple PCF geometry is developed for the biosensing applications. A circular-shaped core is considered to form the PCF core for minimizing fabrication complexity. The hollow core which is circular-shaped is constructed to enhance the interactive area of the targeted substance and light intensity. Alongside, it also helps to minimize the background material requirement that also facilitates reduction in absorption loss. Most of the previously developed PCF geometry is considered nearly 300 μm in core diameter and 3000 μm in total diameter of the sensor to investigate in the THz spectrum in case of sensing [7, 26, 28, 32–36]. For comparison of our investigated results with previously designed PCF, a 3000 μm total sensor diameter with a PML of 250 μm has been considered. 160 μm core radius r_c is considered as optimum after setting the core size at several points in the range of 145 μm to 175 μm. The core hole radius is indicated by r_h which is fixed at 152.5 μm considering the strut width of 7.5 μm. At the abovementioned geometrical conditions, the developed PCF exhibits improved sensing properties such as sensitivity, confinement loss, dispersion, effective material loss, etc. The optimized geometrical parameters are listed in Table 1. Strut width can be defined here as the material width between the core hole and the cladding hole. The strut in the cladding area indicates that the separation area between two adjacent holes is also considered the same as the core strut. A symmetrical circular manner 60° sectoring cladding structure is designed considering the fabrication complexity. Targeted stuff concentration has been applied in the core hole, and dry air is considered in the cladding holes for this investigation. Note that a small size sectoring angle will increase the number of cladding holes with lower dimensions which will increase the complexity due to the higher number of holes that need to be implemented with lower dimensions. On the other hand, a higher sectoring angle will minimize the number of holes in the cladding with large dimensions that will decrease the mechanical strength of the fiber. The lower size of the sectoring angle will increase the material requirements and enhance the material absorption probability which will slightly affect the sensitivity. Considering all the mentioned above, we have achieved better results at a 60-degree sectoring cladding structure considering all the necessary optical properties evaluated in this literature.

Usually, several polymer materials can be strong candidates as host material. Because of a higher absorption loss of polymethyl methacrylate (PMMA) and teflon, these are not considered in this case. Zeonox and Topas are the two-dominant postulants in this area with similar absorption losses (~0.2 cm^{-1}), high glass transition points, high light transmission (91%), avoidable material dispersion, material insensitivity, etc. [37]. As per the experimental evaluation of Zeonox and Topas, there are no significant differences between them in almost all the tested properties cases [37, 38]. So, any of these can be well suited for PCF devices. In this investigation, Topas was chosen as background material. For

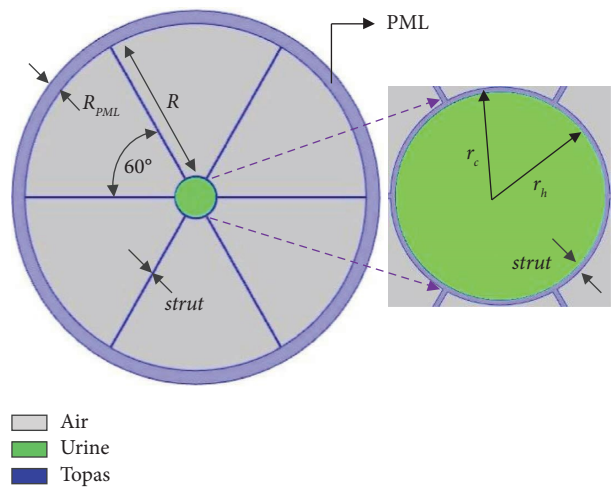

Figure 2: Geometrical cross-sectional view of the proposed PCF with amplified core.

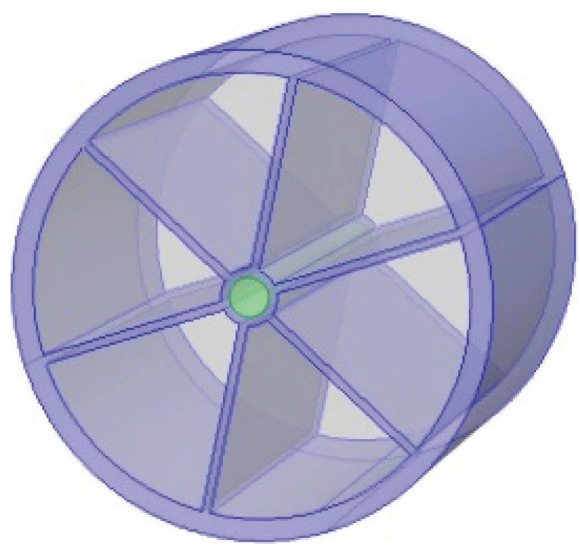

Figure 3: 3D view of the proposed PCF geometry.

Table 1: Optimum geometrical parameters.

Parameters	Dimension (μm)
Core hole radius (r_h)	152.5
Core radius (r_c)	160
Cladding radius (R)	1090
Strut	7.5
PML radius (R_{PML})	250
Total PCF diameter	3000

absorbing the incident radiation produced by the light source, a perfectly matched layer has been used as an antireflecting layer in the outer region of the fiber.

3. Results and Discussions

To design the PCF geometry and analyze the sensing properties of the developed PCF, the most powerful computational technique, the finite element method has been utilized in the COMSOL Multiphysics v. 5.3a environment. Because of its lower computational time and complexity, PDE solution ability makes it the best of the other techniques for optical devices. Several steps are involved in the designing, and analysis of the proposed PCF sensor which is shown in Figure 4. At first, global variables (GVs) and structure variables (SVs) were specified in the Comsol software. After that, the geometry of the PCF was designed as per the plan. The materials of the different parts of the PCF were assigned such as topas in the strut, air in the cladding holes, and targeted analytes in the core section. The PCF meshed after setting the boundary and initial conditions for solving the differential equations. The resulting optical parameter data was collected and exported into the MATLAB software for further analysis. Necessary optical property data was observed and investigated to determine the relationship between frequency and different optical properties. If the results were not satisfactory, geometrical specifications were adjusted to the GVs and SVs, and the process was repeated until a satisfactory or desired outcome was attained. For attaining better accuracy extra-fine element size is maintained in the simulation process. The partial meshing condition of the proposed PCF is shown in Figure 5. The complete mesh of the proposed geometry consists of 46992 domain elements and 2830 boundary elements with a minimum element quality of 0.4599.

The interactive situation of targeted substances, and light intensity is presented in Figure 6 with the intensity scale in x-polarization mode. Because of the symmetrical arrangement in the cladding region with hollow core settlement both polarization modes render the same behavior. From this figure, it is clearly visualized that the interactive area is closely localized in the core area, and the light pulse and targeted substance have strongly interacted. Contrariwise, inconsequential interaction in the cladding region is noticed.

The refractive index of a substance is defined as the ratio of the velocity of light in a vacuum to the velocity of light in a certain bulk medium for a particular frequency. It is noticeable that there is no significant difference between the refractive index (RI) and the effective refractive index (ERI). Only the basic distinction for ERI is the ratio of the speed of light in a vacuum to the speed of light in the bulk media for a certain polarization in the direction of propagation in the guiding phenomenon. The effective refractive index can be estimated by the following expression [7].

$$n_{\mathrm{eff}_{pm}} = \frac{c}{v_{\mathrm{zpm}}} = \frac{\lambda_0 v}{\lambda_{\mathrm{zpm}} v} = \frac{\lambda_0}{\lambda} = \frac{(2\pi/k_0)}{(2\pi/k_0)} = \frac{k_{\mathrm{zpm}}}{k_0} = \frac{\beta_{pm}}{k_0}, \quad (1)$$

where β_{pm} is the propagation constant for a given mode and polarization, p is termed as the polarization (TE or TM), and m is the mth mode of the given polarization, while the wavenumber (k_0) in free space for a particular frequency is found by $k_0 = w/c = 2\pi v/c = 2\pi/\lambda_0$, where λ_0 denotes the wavelength in free space, and v the frequency in all media.

On the basis of the core cladding refractive index, the refractometric PCF biosensor can sustain the light-matter interaction either by the photonic bandgap (PBG) technique or by the modified total internal reflection (MTRI) process. Because of the choise of suspended cladding with a higher air filling fraction and hollow-type core in this proposed work, the light-matter interaction is maintained by the PGB process in this case.

The response of the effective refractive index of the proposed PCF for different levels of albumin concentration in urine with respect to frequency is presented in Figure 7. In general, in the THz regime, the effective refractive index of PCF devices increases with the augmentation of frequencies that facilitates higher optical power interaction. The presented ERI response of the proposed PCF also exhibits the same manner, and this kind of behavior enhances higher-sensitivity responses.

The relative sensitivity is the key property of a sensor to assess the sensing performances of a PCF-based sensing device. The relative sensitivity coefficient expresses a clear notion about the interaction of light with the targeted samples. The amount of light-matter interaction is measured by the absorption coefficient at a certain frequency. The main concern for evaluating the sensing performance of the proposed PCF is to calculate the relative sensitivity. It can be expressed by the following equation [7]:

$$r = \frac{n_r}{n_{\mathrm{eff}}} \times p, \quad (2)$$

where n_r is the refractive index of the targeted analyte (here, $n_r = 1.335$ for 7–125 mg/dl, $n_r = 1.336$ for 250–500 mg/dl, $n_r = 1.337$ for 1000 mg/dl) [2, 37], n_{eff} is the modal refractive index, and the relative sensitivity coefficient is expressed by r and p is the amount of light-matter interaction. It is calculated by [7]

$$p = \frac{\int_{\mathrm{sample}} R_e\left(E_x E_y - E_y H_x\right)\mathrm{dxdy}}{\int_{\mathrm{total}} R_e\left(E_x H_y - E_y H_x\right)\mathrm{dxdy}} \times 100, \quad (3)$$

where E_x and E_y and H_x and H_y are the electric field and magnetic field components, accordingly.

The sensing capability of the developed PCF for protein identification as a function of frequency is presented in Figure 8. Three concentration levels of protein in urine are considered for evaluating the sensitivity of the proposed PCF. The proportion of sensitivity mostly depended on the refractive index of targeted analytes at a fixed design parameter and a certain operating region. Changes of the refractive index for different concentration levels are very tiny, as a result, the rate of sensitivity seems to be the same for all the samples. But the deviations are shown in the enlarged view of the figure. With the augmentation of

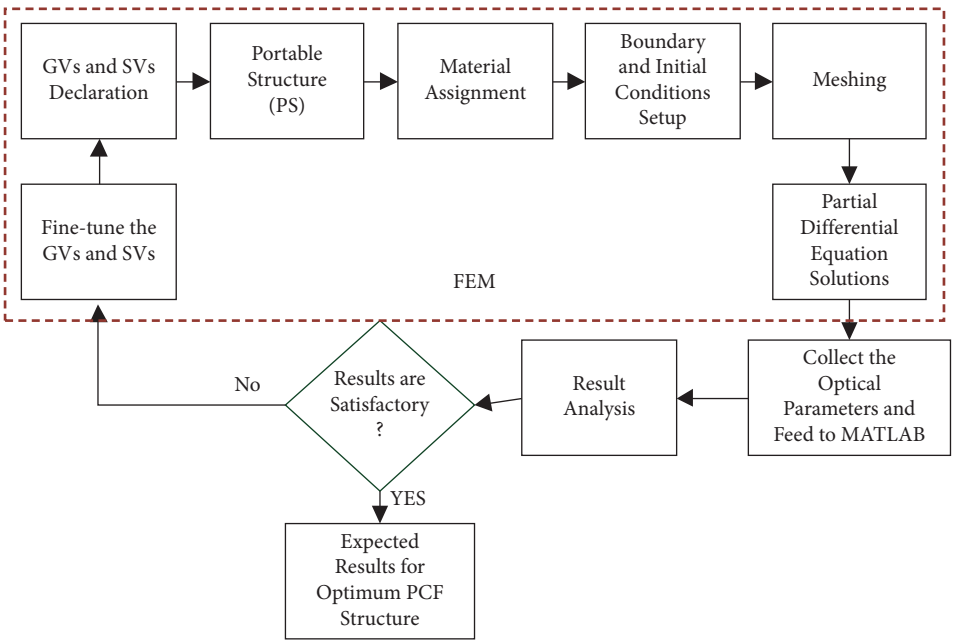

Figure 4: Step-by-step process involved in designing and analyzing of this study.

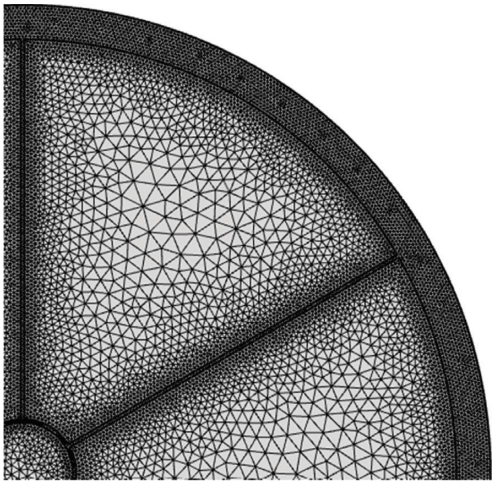

Figure 5: Mesh condition of the proposed PCF.

frequency, light intensity strongly interacts with the targeted analytes which enhances the sensitivity. At a certain frequency, the light-matter interaction reaches its maximum level, after that the sensitivity starts to decline. It can be clearly explained that from Figure 8, at 4.3 THz operating points, the proposed PCF renders maximum sensitivity, and the proportion is 98.576% for 7–125 mg/dl albumin concentration, 98.591% for 250–500 mg/dl, and 98.607% for 1000 mg/dl concentration which is better than many of the existing works for similar application. On an average, the proposed PCF sensor exhibits 10% higher sensitivity than available in the recent literature [6, 7, 26–31].

Sensing performances can be controlled by regulating the geometrical parameters. The sensitivity of the presented PCF for protein detection by changing the core radius and strut size is shown in Figures 9 and 10, respectively. A higher core size raises the possibility of a light interaction area with the matter which helps to improve the sensing response. On the other hand, the descending values of strut have a similar impact in improving the sensitivity. The scenario of these observations is nicely visualized in Figures 9 and 10. Very insignificant sensitivity variations of 0.1% are observed compared to the optimum conditions for every 5 μm core radius changes. On the contrary, nearly 0.75% sensitivity is varied for each 1.5 μm strut size change. Alongside, it is a reality that during fabrication, maintaining an exact optimum geometrical situations is a big challenge. Considering this fact, the sensitivity of presented PCF for protein detection in urine concentration is listed in Table 2 by changing ±2% and ±5% geometrical parameters. It can be expressed

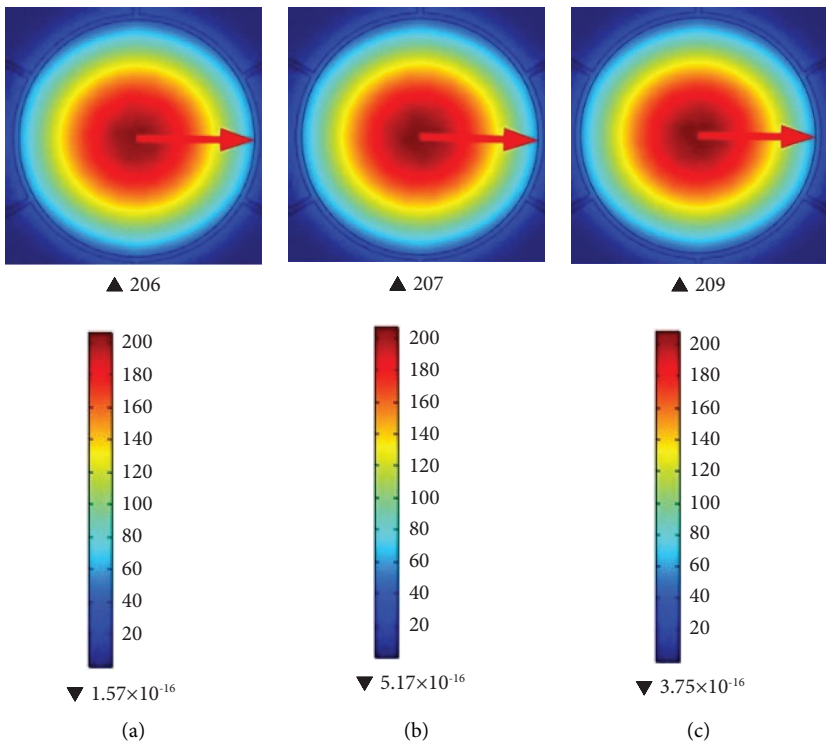

Figure 6: The mode field distribution with intensity scale of the proposed PCF for different levels of protein concentration in x-polarization mode at optimum design conditions (a) 7–125 mg/dl, (b) 250–500 mg/dl, and (c) 1000 mg/dl.

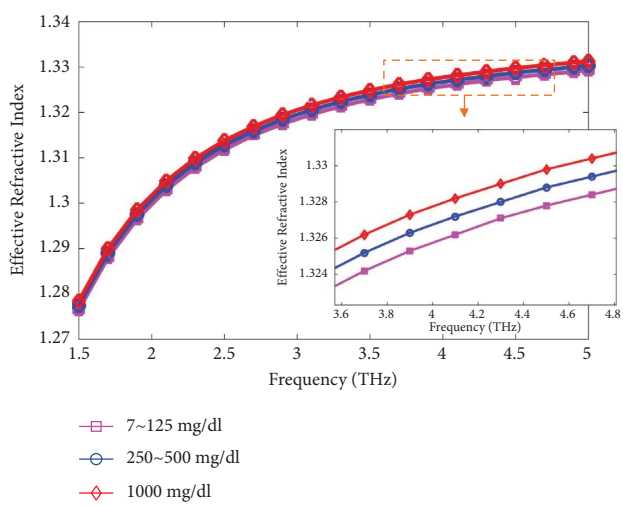

Figure 7: Effective mode profile for different protein concentrations of urine as a function of frequency.

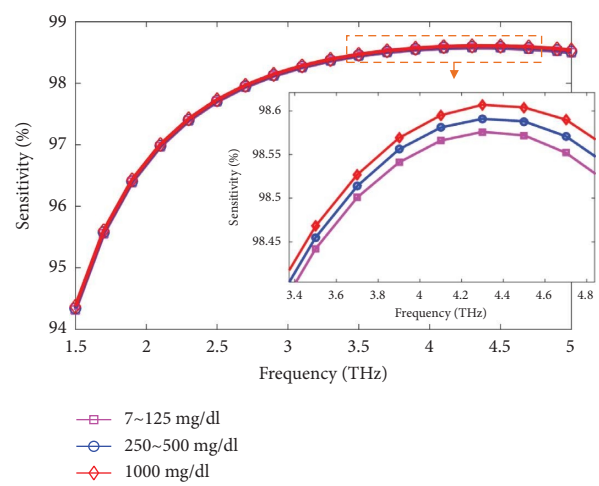

Figure 8: The response of sensitivity to different protein concentrations of the urine as a function of frequency.

that from Table 2, the impact of these geometrical variations on sensitivity is very insignificant. The subtlety of geometries can be varied up to 5% without any significant consequences.

Confinement loss (CL) is another crucial parameter of the optical device in biosensing applications. It is the competency of the sensor to resist the optical power spreading within the nominated low-loss core region. CL arises from the imperfection of the geometrical structure and the leaky nature of the modes, calculated by the imaginary part of the propagation constant as [7, 32, 34].

$$L_c = \left(\frac{4\pi f}{c}\right) Im\left(n_{\text{eff}}\right), cm^{-1}, \tag{4}$$

where c stands for light velocity in vacuum, and $Im(n_{eff})$ specifies the complex part of the propagation mode, and f is the working frequency.

Dispersion is one of the momentous parameters for the optical properties, which is a quantitative analysis of the spreading light pulses when the light pulses have interacted through an optical fiber. The dispersion property of a fiber can be characterized by the following equation [27, 36]:

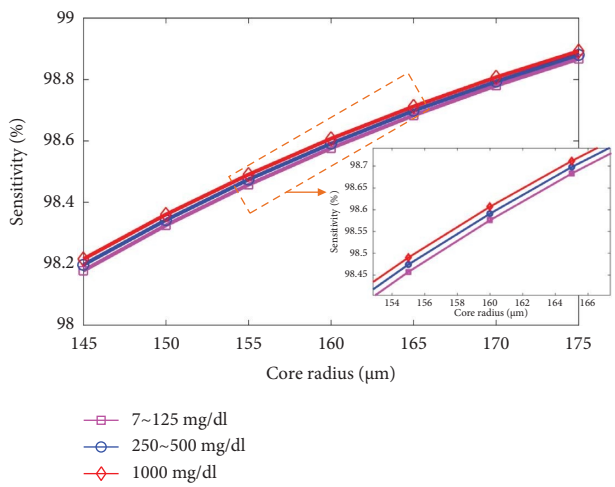

Figure 9: The response of sensitivity for different protein concentrations of the urine with respect to the core radius.

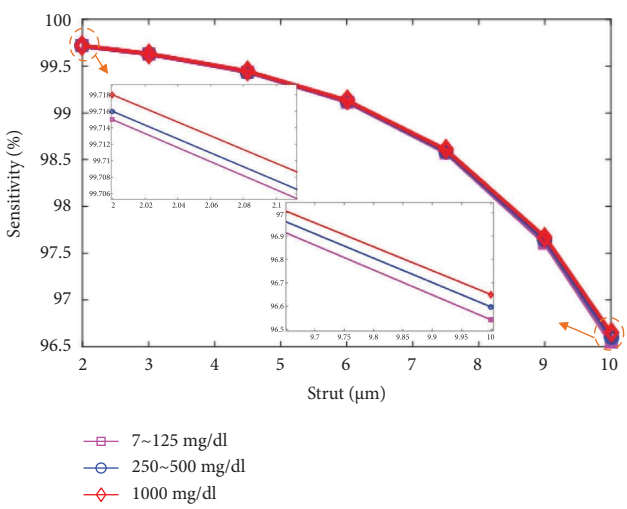

Figure 10: The response of sensitivity to different protein concentrations of the urine with respect to strut width.

$$\beta_2 = \frac{2}{c}\frac{dn_{\text{eff}}}{d\omega} + \frac{\omega}{c}\frac{d^2 n_{\text{eff}}}{d\omega^2}, \tag{5}$$

where ω is the angular frequency, β_2 is the dispersion parameter, and η_{eff} is the effective refractive index of the material.

The variations of confinement loss for different concentrations of albumin have been demonstrated in Figure 11 with the shifting frequency. Due to the ascending manner of frequency, the propagated optical signal compactly passes inside the core region that has an impact on increasing sensitivity. It indicates that when the frequency acts in an incremental nature, the mode fields constrict more strictly towards the hollow core area, and hence, the CL curves exhibit a descending nature for the high level of frequency that neatly signifies in Figure 11. At optimal frequency conditions, the CL is investigated at $8.3 \times 10^{-16}\,\text{cm}^{-1}$, $1.07 \times 10^{-16}\,\text{cm}^{-1}$, and $3.37 \times 10^{-17}\,\text{cm}^{-1}$ for (7–125 mg/dl), (250–500 mg/dl), and 1000 mg/dl concentrations of albumin in urine accordingly which are trivial as compared to the recently proposed RI-dependent sensors for similar application in the PCF platform [5–8, 26–31].

The response of fiber dispersion for each concentration level of the analyte with an ascending frequency is shown in Figure 12 at the optimal design parameters. It can be observed that the resulting dispersion property of the proposed PCF meets a flattening region with a broad-spectrum range of 3.1 THz to 5 THz which is suitable for multichannel sensing applications. The investigated dispersion curves show a very tiny deviation for each concentration level of the sample due to the infinitesimal change of RI. It is also clearly visualized from Figure 12. At the optimal design conditions, a very near-zero dispersion of 0.039 ps/THz/cm is obtained with a dime variation of nearly ±0.032 ps/THz/cm for all the tested concentrations. The obtained dispersion by the proposed PCF sensor is highly comparable with many of the existing works for similar applications due to proper geometry selection and proper geometry optimization [7, 26, 35].

A comparison with the recently developed PCF-based THz sensor for biosensing application is presented in Table 3. It can be mentioned that from Table 3 that this proposed work not only improved the sensitivity, besides all other necessary optical properties have improved at a significant level including confinement loss, effective area, and effective material loss. The hollow core with circular-shaped PCF has a greater interactive area that enhances the interaction area between the applied analyte and light intensities. Besides, the highly porous structure of the cladding and hollow core reduces the interactive area of the light pulse with bulk material, which also helps to reduce losses. Depending on these matters, we have chosen a hollow and circular-shaped core with highly porous cladding geometry. The listed previous works in Table 3 have not considered the above-mentioned two factors together, that makes our developed structure unique with improved performances.

Recently, surface plasmon resonance- (SPR-) based PCF sensors have been reported, showing noticeable changes in outputs for small changes of refractive index among different analytes [9–14]. Resonance wavelength and peak confinement loss are very sensitive to RI of the analytes in the SPR-PCF platform [9–14]. As a result, a slight change in RI of the analytes forces to the resonance wavelength to shift right or left and the peak of the confinement loss to higher or lower level [9–14]. Thus, it could be easier to identify the unknown analyte with very tiny changes in RI using SPR-based PCF sensor. Therefore, SPR-based PCF sensor development and analysis for the identification of different analytes can be a potential research area.

4. Fabrication Feasibilities and Potential Experimental Setup of the Proposed PCF

Fabrication complexity minimization in a proper geometrical setting is a key challenge for PCF development. Keeping that in mind, symmetrical cladding and hollow-core PCF are proposed in this research. The circular hole is

Table 2: Sensitivity of each tested sample at ±2% and ±5% geometric parameter deviation with the optimum design condition at 4.3 THz frequency.

Geometrical parameters	Sensitivity (%)		
	7–125 mg/dl concentration	250–500 mg/dl concentration	1000 mg/dl concentration
+5%	98.581	98.596	98.612
+2%	98.577	98.592	98.608
Optimum	98.576	98.591	98.607
−2%	98.574	98.589	98.603
−5%	98.565	98.580	98.594

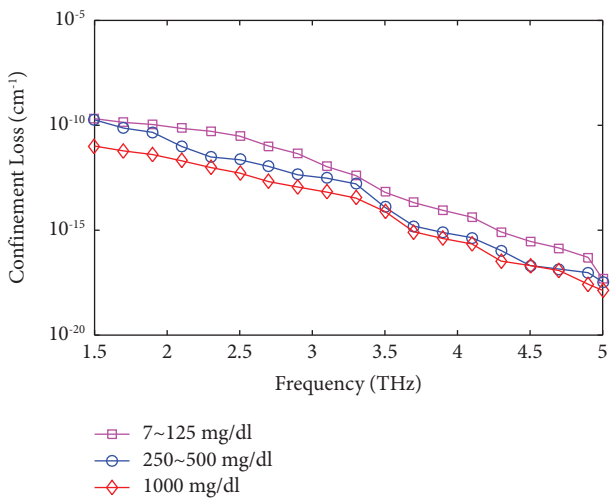

Figure 11: Nature of confinement loss with respect to frequency for different concentrations levels of albumin in urine at optimum design conditions.

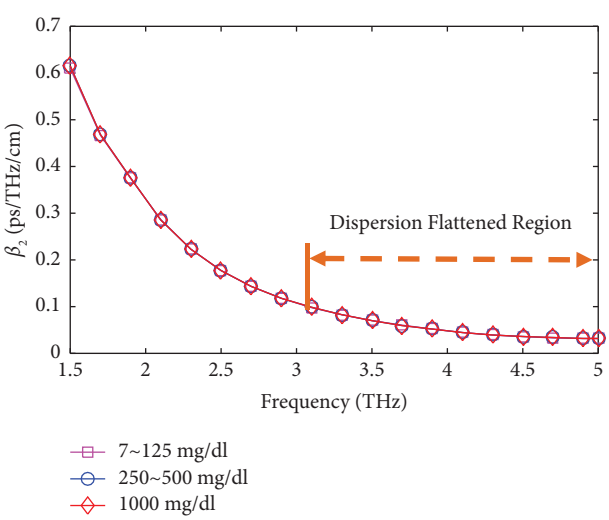

Figure 12: The behavior of the dispersion profile of the proposed PCF for different protein concentrations in the urine as a function of frequency.

comparatively easily implementable by all the existing fabrication processes. It is interesting to note that Bise and Trevor already executed a PCF geometry with a circular airhole structure using sol-gel techniques [39]. Besides this, stack and draw [40], capillary stacking [41], and mechanical drilling [42], are also highly capable of implementing circular hole-structured PCF. Recently, different geometrical structure implementation possibilities are discussed including suspended structure using drilling, stacking, extrusion, and 3D printing techniques [43–49]. Talataisong et al. [45] implemented a suspended structured polymer PCF by using a 3D printing technique. Different complicated PCF geometries including suspended ones have also been fabricated by Cubillas et al. [46]. Lui et al. [47] have fabricated a suspended PCF structure in the stack and draw environment. Furthermore, several complex structures such as kagome and suspended PCF structure have been implemented by Calcerrada et al. [48]. By using the stack and draw fabrication process, different PCF geometries have been also fabricated by Lui et al. [49]. The abovementioned discussions indicate that at this stage, circular holes and suspended cladding structured PCF fabrication is not a complex task. Based on this a fabrication-friendly circular hollow core with suspended cladding-structured PCF is proposed which is easily fabricable on the many existing manufacturing platforms.

For our proposed structure, the stack and draw technique has excellent potential for fabricating the proposed PCF structure. The proposed PCF is constructed with six symmetrical capillaries in the cladding and a circular hollow structure in the core section. Fabrication steps for the proposed PCF using the stack and draw technique are shown in Figure 13. As per the stack and draw process, the first step is capillary preparation. After making solid rod capillaries, an ultrasonic mill can be used for making holes as per the desired shape. After making the cladding capillaries as per the design, these capillaries need to be stacked together inside a jacket tube. After inserting the preform stack into a glass tube and fusing during the drawing process, one obtains a microstructured preform or "cane." The last step of this fabrication process is drawing the cane into fiber as per the design and desired dimension. Air holes size and their regularities can be controlled by applying air pressure inside the preform.

For testing the proposed PCF sensor in practice several additional arrangements are required. A possible arrangement for testing the PCF sensor is presented in Figure 14. First, a supercontinuum light source is required which has a frequency range of 1.5–5 THz. For this purpose, a SuperK compact, NKTPhotonics™ can be utilized [50]. A single-mode fiber (SMF-28) needs to be coupled between the light source and sensor through the polarizer (which is accompanied by a polarizer controller)

Table 3: Comparison with recent RI-dependent sensors for similar application in the PCF platform.

Ref.	Targeted analyte/s	Refractive index	Sensitivity (%)	Lc	β_2 (ps/THz/cm)	EML (cm^{-1})	A_{eff}
[6]	Sarin, soman, and tabun	1.366–1.44	92.84–94.4	1.71×10^{-14} cm^{-1}	—	0.0085–0.0094	—
[7]	Water, plasma, WBCs, hemoglobin, and RBCs	1.33–1.4	79.39–80.93	$10^{-10\pm1}$ (dB/cm)	2.1 ± 2.02		$\approx 1 \times 10^5$ (μm^2)
[26]	Water, plasma, WBCs, hemoglobin, and RBCs	1.33–1.4	89.14–93.50	$10^{-13.5\pm0.5}$ (cm^{-1})		—	2.2×10^5 μm^2
[27]	Bilirubin	—	95	2.64×10^{-15} (dB/cm)	—	0.0013	—
[28]	Plasma, WBCs, hemoglobin, and RBCs	1.33–1.4	84.55–85.09	$10^{-9\pm0.5}$ (cm^{-1})	—	—	1.86×10^{-7} m^2
[29]	Dioxin, toluene, hydrogen sulfide, nitrogen dioxide, and sodium cyanide	1.36–1.65	89.6–91.5	$10^{-16\pm1}$ (cm^{-1})	—	0.019 ± 0.001	$(4\text{-}5) \times 10^{-8}$ m^2
[30]	Blood serum and blood plasma	1.3561–1.3564	66.7–73.4	$1.55 \times 10^{-12\pm1}$ (cm^{-1})	2.6×10^{-3}	0.212–0.217	(6.1–6.4) μm^2
Proposed work	Albumin	**1.335–1.337**	**98.58–98.61**	**$10^{-16.5\pm0.5}$ (cm^{-1})**	**0.30 ± 0.33**	**≈0.0173**	**$\approx 5.06 \times 10^{-8}$ m^2**

Performances of proposed works are highlighted by bold values.

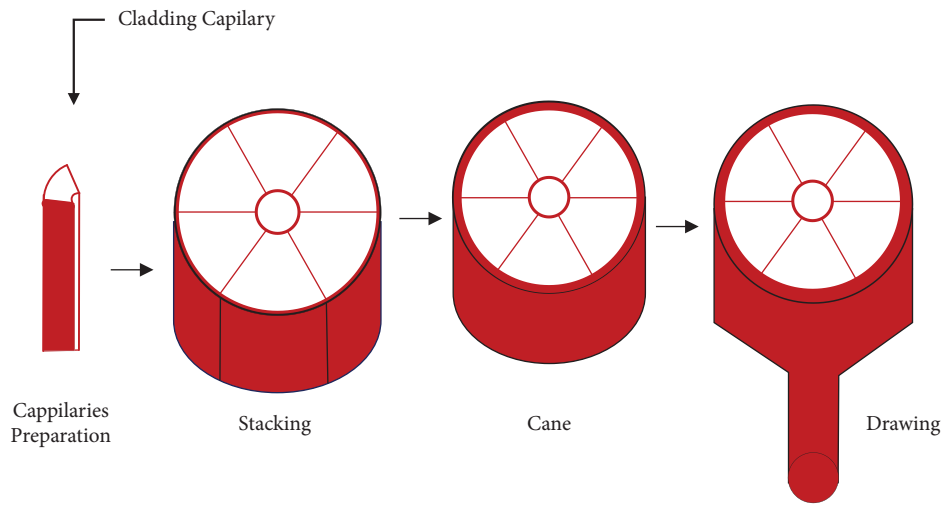

Figure 13: Fabrication processing steps for the proposed PCF using the stack and draw technique.

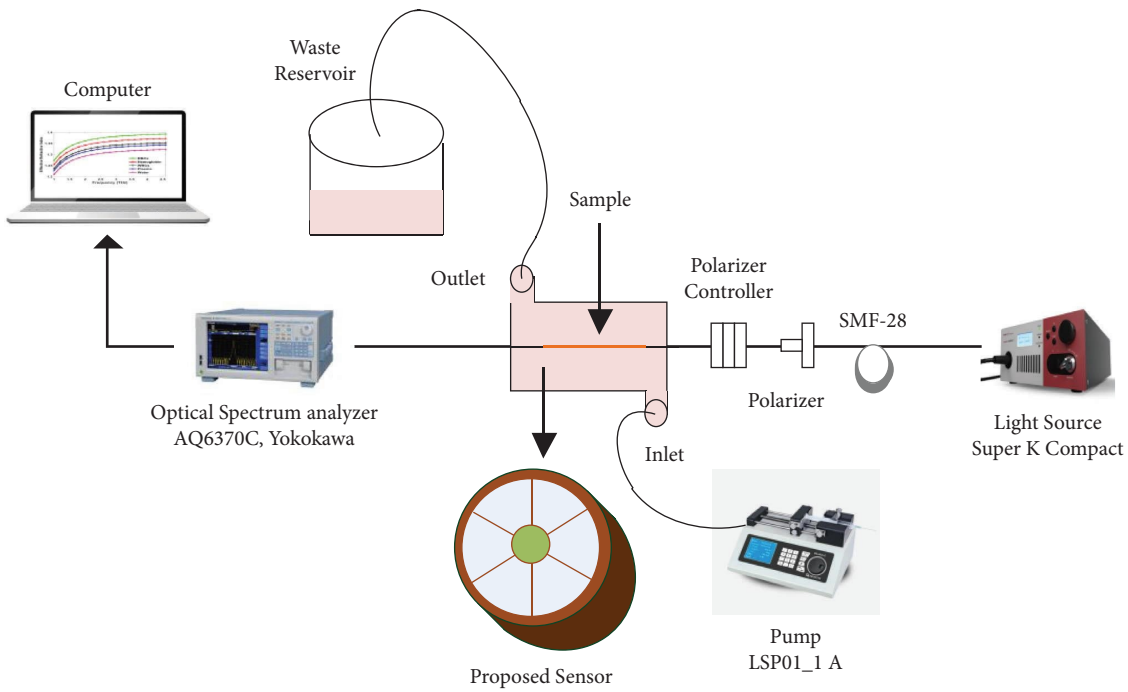

Figure 14: Experimental setup schematic of proposed PCF sensors for practical sensing applications.

to transport the light to the sensor. A splicing method can be used to couple the sensor with SMF-28. The Vytran FFS-2000 splicer can be utilized for splicing by using the filament fusion technique. Manual-mode translational and rotational alignment methods can be used for aligning the PCF and SMF [51]. Furthermore, SMF and PCF can also be connected by inserting an etched SMF tip into the PCF. As per the current reports, this splicing method has a coupling efficiency of more than 80% [52]. Also, free-space coupling, fiber-to-fiber coupling, etc. techniques can be also utilized for coupling purposes [53, 54]. After passing the sensor, the light needs to pass through an optical spectrum analyzer which analyzes the responses of different analytes. Yokokawa™, AQ6370C optical spectrum analyzer can be employed [50]. For injecting the analyte into the sensor, a programmable microinjector pump would be required. LongerPump™, LSP01-1A can be considered for this purpose [50]. A waste reservoir needs to be connected with an outlet channel where the used analyte will be stored. The existence of several unknown analytes causes peak shifts. These shifts can be identified by the spectrum analyzer and can be graphically displayed on the computer which will be connected to the output of the spectrum analyzer.

5. Conclusion

In this research, a refractive index-based hollow-core PCF biosensor has been proposed for albumin detection in urine on the basis of kidney dysfunctionality identification. To investigate the sensing performance of the presented PCF, three levels of protein concentration in urine have been considered. The investigated consequence of the proposed PCF reveals a superior relative sensitivity response of 98.576% for 7–125 mg/dl albumin concentration, 98.591% for 250–500 mg/dl, and 98.607% for 1000 mg/dl concentration in the terahertz spectrum. Moreover, it renders a very trivial confinement loss and a near-zero dispersion flattened profile. The investigated results of the proposed PCF and the practical implementation feasibility of state-of-the-art fabrication technology apprise that it can be a great solution for biosensing applications.

Data Availability

Data are not available anywhere. All the supporting data are reserved at the author's end.

Conflicts of Interest

The authors declare that they have no conflicts of interest regarding the publication of this paper.

References

[1] J. C. Seegmiller, W. G. Miller, and L. M. Bachmann, "Moving toward standardization of urine albumin measurements," *The Journal of the International Fedaration of Clinical Chemistry and Laboratory Medicine*, vol. 28, no. 4, pp. 258–267, 2017.

[2] S. I. Ahmad, S. Ahmed, I. A. Syed, S. A. Ansari, and A. Ahmad, "Rheological and infrared spectroscopic investigations of normal and chronic kidney disease urine," *Oriental Journal of Chemistry*, vol. 32, no. 3, pp. 1421–1431, 2016.

[3] M. S. Islam, J. Sultana, S. Rana et al., "Extremely low material loss and dispersion flattened TOPAS based circular porous fiber for long distance terahertz wave transmission," *Optical Fiber Technology*, vol. 34, pp. 6–11, 2017.

[4] Z. Wu, Z. Shi, H. Xia et al., "Design of highly birefringent and low-loss oligoporous-core THz photonic crystal fiber with single circular air-hole unit," *IEEE Photonics Journal*, vol. 8, no. 6, Article ID 4502711, p. 11, 2016.

[5] M. S. Islam, J. Sultana, A. A. Rifat, A. Dinovitser, B. Wai-Him Ng, and D. Abbott, "Terahertz sensing in a hollow core photonic crystal fiber," *IEEE Sensors Journal*, vol. 18, no. 10, pp. 4073–4080, 2018.

[6] M. B. Hossain, E. Podder, A. A. M. Bulbul, and H. S. Mondal, "Bane chemicals detection through photonic crystal fiber in THz regime," *Optical Fiber Technology*, vol. 54, Article ID 102102, 2020.

[7] K. Ahmed, F. Ahmed, S. Roy et al., "Refractive index based blood components sensing in terahertz spectrum," *IEEE Sensors Journal*, vol. 19, no. 9, pp. 3368–3375, 2019.

[8] M. S. Islam, J. Sultana, K. Ahmed et al., "A novel approach for spectroscopic chemical identification using photonic crystal fiber in the terahertz regime," *IEEE Sensors Journal*, vol. 18, no. 2, pp. 575–582, 2018.

[9] K. Ahmed, R. Amin, F. M. Bui et al., "Design and analysis of multi-analyte detection based biosensor in the visible to near-infrared (VNIR) region," *IEEE Transactions on Nano-Bioscience*, vol. 31, p. 1, 2023.

[10] K. Ahmed, F. M. Bui, and F. X. Wu, "PreOBP_ML: machine learning algorithms for prediction of optical biosensor parameters," *Micromachines*, vol. 14, no. 6, p. 1174, 2023.

[11] S. Singh and Y. K. Prajapati, "Novel bottom-side polished PCF-based plasmonic biosensor for early detection of hazardous cancerous cells," *IEEE Transactions on Nano-Bioscience*, vol. 22, no. 3, pp. 647–654, 2023.

[12] R. Srivastava, Y. K. Prajapati, S. Pal, and S. Kumar, "Micro-Channel Plasmon sensor based on a D-shaped photonic crystal fiber for malaria diagnosis with improved performance," *IEEE Sensors Journal*, vol. 22, no. 15, pp. 14834–14841, 2022.

[13] S. Singh and Y. K. Prajapati, "Antimonene-gold based twin-core SPR sensor with a side-polished semi-arc groove dual sensing channel: an investigation with 2D material," *Optical and Quantum Electronics*, vol. 54, no. 2, p. 114, 2022.

[14] S. Singh and Y. K. Prajapati, "Highly sensitive dual-core symmetrical side-polished modified D-shaped SPR based PCF refractive index sensor with deeply etched micro openings," *Optik*, vol. 235, Article ID 166657, 2021.

[15] M. M. A. Eid, M. A. Habib, M. S. Anower, and A. N. Z. Rashed, "Highly sensitive nonlinear photonic crystal fiber based sensor for chemical sensing applications," *Microsystem Technologies*, vol. 27, no. 3, pp. 1007–1014, 2021.

[16] B. K. Paul, E. Rajesh, S. Asaduzzaman et al., "Design and analysis of slotted core photonic crystal fiber for gas sensing application," *Results in Physics*, vol. 11, pp. 643–650, 2018.

[17] M. R. Islam, A. N. M. Iftekher, F. A. Mou, M. M. Rahman, and M. I. H. Bhuiyan, "Design of a Topas-based ultrahigh-sensitive PCF biosensor for blood component detection," *Applied Physics A*, vol. 127, no. 2, p. 109, 2021.

[18] B. M. Fischer, M. Hoffmann, H. Helm et al., "Terahertz time-domain spectroscopy and imaging of artificial RNA," *Optics Express*, vol. 13, no. 14, pp. 5205–5215, 2005.

[19] A. G. Markelz, A. Roitberg, and E. J. Heilweil, "Pulsed terahertz spectroscopy of DNA, bovine serum albumin and collagen between 0.1 and 2.0 THz," *Chemical Physics Letters*, vol. 320, no. 1-2, pp. 42–48, 2000.

[20] M. Nagel, P. Haring Bolivar, M. Brucherseifer, H. Kurz, A. Bosserhoff, and R. Büttner, "Integrated THz technology for label-free genetic diagnostics," *Applied Physics Letters*, vol. 80, no. 1, pp. 154–156, 2002.

[21] C. Yu, S. Fan, Y. Sun, and E. Pickwell-MacPherson, "The potential of terahertz imaging for cancer diagnosis: a review of investigations to date," *Quantitative Imaging in Medicine and Surgery*, vol. 2, no. 1, pp. 33–45, 2012.

[22] H. Y. Fu, H. Y. Tam, L. Y. Shao et al., "Pressure sensor realized with polarization-maintaining photonic crystal fiber-based Sagnac interferometer," *Applied Optics*, vol. 47, no. 15, pp. 2835–2839, 2008.

[23] C. M. Jewart, S. M. Quintero, A. M. B. Braga, and K. P. Chen, "Design of a highly-birefringent microstructured photonic crystal fiber for pressure monitoring," *Optics Express*, vol. 18, no. 25, pp. 25657–25664, 2010.

[24] B. Kuiri, B. Dutta, N. Sarkar et al., "Design and optimization of photonic crystal fiber with low confinement loss guiding 98 OAM modes in THz band," *Optical Fiber Technology*, vol. 68, Article ID 102752, 2022.

[25] B. Kuiri, B. Dutta, N. Sarkar et al., "Ultra-low loss polymer-based photonic crystal fiber supporting 242 OAM modes with

high bending tolerance for multimode THz communication," *Results in Physics*, vol. 36, Article ID 105465, 2022.

[26] M. B. Hossain and E. Podder, "Design and investigation of PCF-based blood components sensor in terahertz regime," *Applied Physics A*, vol. 125, no. 12, p. 861, 2019.

[27] A. R. Elhelw, M. S. S. Ibrahim, A. N. Z. Rashed, A. E.-N. A. Mohamed, M. F. O. Hameed, and S. S. A. Obayya, "Highly sensitive Bilirubin biosensor based on photonic crystal fiber in terahertz region," *Photonics*, vol. 10, no. 1, p. 68, 2023.

[28] A. Kumar, P. Verma, and P. Jindal, "Decagonal solid core PCF based refractive index sensor for blood cells detection in terahertz regime," *Optical and Quantum Electronics*, vol. 53, no. 4, p. 165, 2021.

[29] H. Chopra, R. S. Kaler, and B. Painam, "Photonic crystal waveguide-based biosensor for detection of diseases," *Journal of Nanophotonics*, vol. 10, no. 3, Article ID 036011, 2016.

[30] S. Asaduzzaman, H. Rehana, R. Chakma et al., "Hexa-sectored square photonic crystal fiber for blood serum and plasma sensing with ultralow confinement loss," *Applied Physics*, vol. 128, no. 6, p. 467, 2022.

[31] M. M. Rahman, F. A. Mou, M. I. H. Bhuiyan, and M. R. Islam, "Photonic crystal fiber-based terahertz sensor for cholesterol detection in human blood and liquid foodstuffs," *Sensing and Bio-Sensing Research*, vol. 29, Article ID 100356, 2020.

[32] F. A. Mou, M. M. Rahman, M. R. Islam, and M. I. H. Bhuiyan, "Development of a photonic crystal fiber for THz wave guidance and environmental pollutants detection," *Sensing and Bio-Sensing Research*, vol. 29, Article ID 100346, 2020.

[33] M. R. Islam, F. A. Mou, M. M. Rahman, and M. I. Hassan Bhuiyan, "Hollow core photonic crystal fiber for chemicals sensing in liquid analytes: design and analysis," *International Journal of Modern Physics B*, vol. 34, no. 28, Article ID 2050259, 2020.

[34] M. S. Islam, B. K. Paul, K. Ahmed, and S. Asaduzzaman, "Rhombic core photonic crystal fiber for sensing applications: Modeling and analysis," *Optik*, vol. 157, pp. 1357–1365, 2018.

[35] S. R. Tahhan and H. K. Aljobouri, "Sensing of illegal drugs by using photonic crystal fiber in terahertz regime," *Journal of Optical Communications*, vol. 0, no. 0, 2020.

[36] M. M. Rahman, F. A. Mou, M. I. H. Bhuiyan, and M. R. Islam, "Refractometric THz sensing of blood components in a photonic crystal fiber platform," *Brazilian Journal of Physics*, vol. 52, no. 2, p. 47, 2022.

[37] M. S. Islam, C. M. B. Cordeiro, M. J. Nine et al., "Experimental study on glass and polymers: determining the optimal material for potential use in terahertz technology," *IEEE Access*, vol. 8, pp. 97204–97214, 2020.

[38] K. Nielsen, H. K. Rasmussen, A. J. L. Adam, P. C. Planken, O. Bang, and P. U. Jepsen, "Bendable, low-loss Topas fibers for the terahertz frequency range," *Optics Express*, vol. 17, no. 10, pp. 8592–8601, 2009.

[39] R. T. Bise and D. Trevor, "Solgel-derived micro-structured fibers: fabrication and characterization," in *Proceedings of the Optical Fiber Communication Conference*, pp. 6–11, Anaheim, CA, USA, August 2005.

[40] D. Pysz, I. Kujawa, R. Stepien et al., "Stack and draw fabrication of soft glass microstructured fiber optics," *Bulletin of the Polish Academy of Sciences, Technical Sciences*, vol. 62, pp. 667–682, 2014.

[41] W. Guo, G. Zhou, L. Hou, Y. Han, Q. Li, and Y. Liu, "The fabrication of micro-structure fiber with the improved stacking-capillary method," *Advanced Laser Technologies*, vol. 6344, 2005.

[42] P. Zhang, J. Zhang, P. Yang, S. Dai, X. Wang, and W. Zhang, "Fabrication of chalcogenide glass photonic crystal fibers with mechanical drilling," *Optical Fiber Technology*, vol. 26, pp. 176–179, 2015.

[43] A. Ghazanfari, W. Li, M. C. Leu, and G. E. Hilmas, "A novel freeform extrusion fabrication process for producing solid ceramic components with uniform layered radiation drying," *Additive Manufacturing*, vol. 15, pp. 102–112, 2017.

[44] V. R. Kumar, A. K. George, W. H. Reeves et al., "Extruded soft glass photonic crystal fiber for ultrabroad supercontinuum generation," *Optics Express*, vol. 10, no. 25, p. 1520, 2002.

[45] W. Talataisong, R. Ismaeel, S. R. Sandoghchi et al., "Novel method for manufacturing optical fiber: extrusion and drawing of microstructured polymer optical fibers from a 3D printer," *Optics Express*, vol. 26, no. 24, Article ID 32007, 2018.

[46] A. M. Cubillas, S. Unterkofler, T. G. Euser et al., "Photonic crystal fibres for chemical sensing and photochemistry," *Chemical Society Reviews*, vol. 42, no. 22, pp. 8629–8648, 2013.

[47] Z. Liu, C. Wu, M. L. V. Tse, and H. Y. Tam, "Fabrication, characterization, and sensing applications of a high-birefringence suspended-core fiber," *Journal of Lightwave Technology*, vol. 32, pp. 2113–2122, 2014.

[48] M. Calcerrada, C. García-Ruiz, and M. González-Herráez, "Chemical and biochemical sensing applications of microstructured optical fiber-based systems," *Laser & Photonics Reviews*, vol. 9, no. 6, pp. 604–627, 2015.

[49] Z. Liu and H. Y. Tam, "Fabrication and sensing applications of special microstructured optical fibers," *Selected Topics on Optical Fiber Technologies and Applications*, Intech, Houston, TX, USA, 2018.

[50] Z. Liu, Y. Wei, Y. Zhang et al., "Reflective-distributed SPR sensor based on twin-core fiber," *Optics Communications*, vol. 366, pp. 107–111, 2016.

[51] L. R. Jaroszewicz, M. Murawski, and K. Stasiewicz, "A photonic crystal fiber splice with a standard single mode fiber," *Photonics Letters of Poland*, vol. 1, no. 3, pp. 115–117, 2009.

[52] D. Fan, Z. Jin, G. Wang et al., "Extremely high-efficiency coupling method for hollow-core photonic crystal fiber," *IEEE Photonics Journal*, vol. 9, no. 3, pp. 1–8, 2017.

[53] V. Parmar, R. Bhatnagar, and P. Kapur, "Optimized butt coupling between single mode fiber and hollow-core photonic crystal fiber," *Optical Fiber Technology*, vol. 19, no. 5, pp. 490–494, 2013.

[54] B. Li, D. Zheng, D. Kong, E. Chen, and J. Wu, "Free space to single mode fiber coupling efficiency improvement using wave-front sensor-less adaptive optics," in *Proceedings of the Asia Communications and Photonics Conference (ACP)*, Wuhan, China, November 2016.